

Compressed Sensing with Invertible Generative Models and Dependent Noise

Jay Whang
jaywhang@cs.utexas.edu
University of Texas at Austin

Qi Lei
leiqi@ices.utexas.edu
University of Texas at Austin

Alexandros G. Dimakis
dimakis@austin.utexas.edu
University of Texas at Austin

April 22, 2022

Abstract

We study image inverse problems with invertible generative priors, specifically normalizing flow models. Our formulation views the solution as the maximum a posteriori (MAP) estimate of the image given the measurements. Our general formulation allows for any differentiable noise model with long-range dependencies as well as non-linear differentiable forward operators. We establish theoretical recovery guarantees for denoising and compressed sensing under our framework. We also empirically validate our method on various inverse problems including compressed sensing with quantized measurements and denoising with highly structured noise patterns.

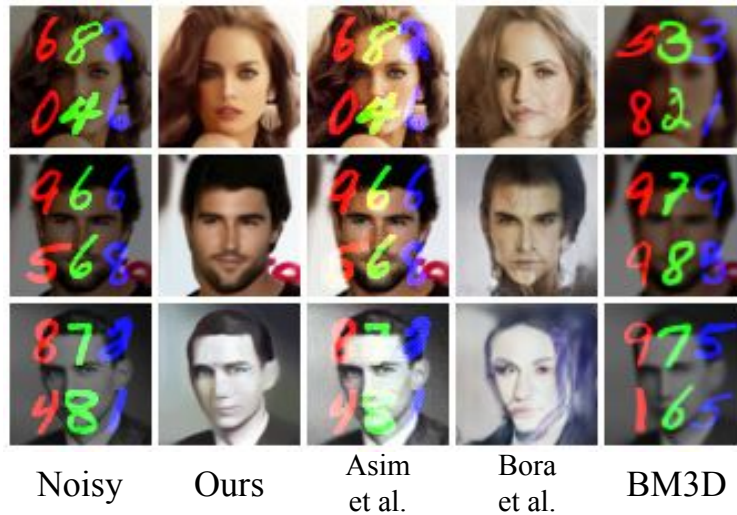


Figure 1: Result of denoising MNIST digits. The first column contains noisy observations, and subsequent columns contain reconstructions.

1 Introduction

Inverse problems seek to reconstruct an unknown signal from observations (or *measurements*), which are produced by some process that transforms the original signal. Because such processes are often lossy and noisy, inverse problems are typically formulated as reconstructing \mathbf{x} from its measurements

$$\mathbf{y} = f(\mathbf{x}) + \delta \tag{1}$$

where f is a known deterministic *forward operator* and δ is an additive noise which may have a complex structure itself. An impressively wide range of applications can be posed under this formulation with an appropriate choice of f and δ , such as compressed sensing [1, 2], computed tomography [3], magnetic resonance imaging (MRI) [4], and phase retrieval [5, 6].

In general for a non-invertible forward operator f , there can be potentially infinitely many signals that match given observations. Thus the recovery algorithm must critically rely on *a priori* knowledge about the original signal to find the most plausible solution among them. Sparsity has classically been a very influential structural prior for various inverse problems [1, 2, 7]. Alternatively, recent approaches introduced deep generative models as a powerful signal prior, showing significant gains in reconstruction quality compared to sparsity priors [8–10].

Contributions

- We present a general formulation for obtaining maximum a posteriori (MAP) estimation reconstructions for dependent noise and general forward operators. Notably, our method can leverage generative models for both the original image and the noise. For linear inverse problems with Gaussian noise, our method reduces to the method of Asim et al. [9].
- We empirically show that our method achieves excellent reconstruction in the presence of noise with various complex and dependent structures. Specifically, we demonstrate the efficacy of our method on various inverse problems with structured non-Gaussian noise and non-linear forward operators.
- We provide the initial theoretical characterization of likelihood-based priors for two common linear inverse problems: denoising and compressed sensing. For denoising, we show a reconstruction error bound that depends on the concavity of the log-likelihood function. For compressed sensing, we further generalize the results of Bora et al. [8] with a random measurement matrix to bound the recovery error under our MAP formulation.

2 Background

2.1 Invertible Generative Models

Invertible generative models, also known as *normalizing flows*, are a class of likelihood-based generative models that allow efficient sampling, inversion and likelihood estimation [11, and references therein]. They approximate complex distributions by mapping a simple noise such as isotropic Gaussian through a differentiable, invertible function G [12]. Sampling procedure is thus $\mathbf{z} \sim p(\mathbf{z}), \mathbf{x} = G(\mathbf{z})$. Since G is invertible, change of variables formula allows us to compute the log-density of \mathbf{x} :

$$\log p(\mathbf{x}) = \log p(\mathbf{z}) + \log |\det J_{G^{-1}}(\mathbf{x})|, \tag{2}$$

where $J_{G^{-1}}(\mathbf{x})$ is the Jacobian of G^{-1} evaluated at \mathbf{x} . Since $\log p(\mathbf{z})$ is a simple distribution, computing the likelihood at any point \mathbf{x} is straightforward as long as G^{-1} and the log-determinant term can be efficiently evaluated.

Notably, the invertibility of G guarantees that it has an unrestricted range and can generate samples that are out-of-distribution, albeit at lower probability. This is a key distinction from a GAN, whose generator

has a restricted range and can only generate samples from the distribution it was trained on. As pointed out by Asim et al. [9] and also shown below in our experiments, this leads to performance benefits on out-of-distribution examples.

2.2 Related Work

We briefly review the existing literature on the application of deep generative models to inverse problems. While vast literature exists on compressed sensing and other inverse problems, the idea of using a deep generative prior was introduced relatively recently by Bora et al. [8]. In that work, the generator from a GAN [13, 14] was shown to be an effective prior for compressed sensing.

Several recent studies have investigated different ways to incorporate deep generative models into inverse problems. Dhar et al. [15] proposed an extension to [8] which expanded the range of the generator by allowing sparse deviations. Similarly, Shah and Hegde [16] proposed another algorithm based on projected gradient descent that extends [8] with theoretical convergence guarantees. Van Veen et al. [10] showed that an *untrained* convolutional neural network can be used as a prior for imaging tasks based on Deep Image Prior by Ulyanov et al. [17].

More recently, Wu et al. [18] applied techniques from meta-learning to improve the reconstruction speed, and Ardizzone et al. [19] showed that by modelling the forward process with a flow model, one can *implicitly* learn the inverse process through the invertibility of the model. Asim et al. [9] proposed to replace the GAN prior of [8] with a normalizing flow model and reported excellent reconstruction performance, especially on out-of-distribution images.

3 Our Method

3.1 Notations and Setup

We use bold lower-case variables to denote vectors, $\|\cdot\|$ to denote ℓ_2 norm, and \odot to denote element-wise multiplication. We also assume the existence of an (unknown) true data distribution $p(\mathbf{x})$, a deterministic and differentiable forward operator f , and a noise distribution p_Δ (which itself can be a generative model). Thus an observation is generated via $\mathbf{y} = f(\mathbf{x}) + \delta$ where $\mathbf{x} \sim p$ and $\delta \sim p_\Delta$.

Note that while f and p_Δ are known, they cannot be treated as fixed across different examples, e.g. in compressed sensing the measurement matrix is random and thus only known at the time of observation.

3.2 MAP Formulation

For a given observation \mathbf{y} , our method tries to recover \mathbf{x} as the maximum a posteriori (MAP) estimate of the conditional distribution $p(\mathbf{x}|\mathbf{y})$:

$$\begin{aligned} \arg \max_{\mathbf{x}} \log p(\mathbf{x}|\mathbf{y}) &= \arg \max_{\mathbf{x}} [\log p(\mathbf{y}|\mathbf{x}) + \log p(\mathbf{x}) - \log p(\mathbf{y})] \\ &\stackrel{(1)}{=} \arg \max_{\mathbf{x}} [\log p_\Delta(\mathbf{y} - f(\mathbf{x})) + \log p(\mathbf{x})] \\ &\triangleq \arg \min_{\mathbf{x}} L_{\text{MAP}}(\mathbf{x}; \mathbf{y}) \end{aligned}$$

where

$$L_{\text{MAP}}(\mathbf{x}; \mathbf{y}) = -\log p_\Delta(\mathbf{y} - f(\mathbf{x})) - \log p(\mathbf{x}). \quad (3)$$

Note that in (1) we drop the marginal density $\log p(\mathbf{y})$ as it is constant and rewrite the conditional $p(\mathbf{y}|\mathbf{x})$ as $p_\Delta(\mathbf{y} - f(\mathbf{x}))$.

Now we approximate the true distribution p with a flow model $p_G(\mathbf{x})$ defined by an invertible mapping G . Recalling that the generative procedure for the flow model is $\mathbf{z} \sim \mathcal{N}(\mathbf{0}, I)$, $\mathbf{x} = G(\mathbf{z})$, we arrive at the following loss function:

$$L_G(\mathbf{z}; \mathbf{y}) \triangleq -\log p_\Delta(\mathbf{y} - f(G(\mathbf{z}))) - \log p_G(G(\mathbf{z})) \quad (4)$$

The invertibility of G allows us to minimize the above loss with respect to either \mathbf{z} or \mathbf{x} :

$$\begin{aligned} \arg \min_{\mathbf{z}} L_G(\mathbf{z}; \mathbf{y}) &= \arg \min_{\mathbf{z}} [-\log p_\Delta(\mathbf{y} - f(G(\mathbf{z}))) - \log p_G(G(\mathbf{z}))] \\ &= \arg \min_{\mathbf{x}} [-\log p_\Delta(\mathbf{y} - f(\mathbf{x})) - \log p_G(\mathbf{x})] = \arg \min_{\mathbf{x}} L_G(\mathbf{x}; \mathbf{y}) \end{aligned}$$

We have experimented with optimizing the loss both in image space \mathbf{x} and latent space \mathbf{z} , and found that the latter achieved better performance across almost all experiments. Since the above optimization objective is differentiable, any gradient-based optimizer can be used to approximately find the minimizer. In practice, even with an imperfect model and approximate optimization, we observe that our approach performs well across a wide range of tasks as shown in the experimental results below.

3.3 Prior Work

This paper generalizes the work of Bora et al. [8] and Asim et al. [9], so we describe the methods proposed in those papers in detail. Importantly, we show that their approaches are special cases of our MAP formulation. Note that both papers considered linear inverse problems, so they correspond to the case where $f(\mathbf{x}) = A\mathbf{x}$ under our notation.

GAN Prior: [8] considers the following loss:

$$L_{\text{Bora}}(\mathbf{z}; \mathbf{y}) = \|\mathbf{y} - A\mathbf{G}(\mathbf{z})\|^2 + \lambda \|\mathbf{z}\|^2, \quad (5)$$

which tries to project the input \mathbf{y} onto the range of the generator G with ℓ_2 regularization on the latent variable. While it looks similar to our loss, this approach is conceptually very different. First, the generator G here is not invertible as it maps a noise to a higher-dimensional vector. This means that the ground truth image we wish to recover may not be in the range of G . The inability to represent any arbitrary image was pointed out by Asim et al. [9] as well, and this does lead to poor reconstruction as our experiments show. Also this formulation does not offer a probabilistic interpretation because GANs generally do not provide likelihood.

Flow Prior: [9] has been the main inspiration for our work. In that paper the authors consider the objective below that tries to simultaneously match the observation and maximize the likelihood of the reconstruction under the model:

$$L(\mathbf{z}; \mathbf{y}) = \|\mathbf{y} - A\mathbf{G}(\mathbf{z})\|^2 - \gamma \log p_G(\mathbf{x}), \quad (6)$$

for some hyperparameter $\gamma > 0$. This loss is a special case of our MAP loss for isotropic Gaussian noise $\delta \sim \mathcal{N}(\mathbf{0}, \gamma I)$, since the log-density of δ becomes $\log p_\Delta(\delta) = -\frac{1}{2\gamma} \|\delta\|^2 - C$ for a constant C . However, Asim et al. [9] report that due to optimization difficulty, they found the following proxy loss to perform better in experiments:

$$L_{\text{Asim}}(\mathbf{z}; \mathbf{y}) = \|\mathbf{y} - A\mathbf{G}(\mathbf{z})\|^2 + \gamma \|\mathbf{z}\|. \quad (7)$$

This is again related to a specific instance of our loss when the flow model is volume-preserving (i.e. the log-determinant term is constant). Continuing from eq. (2): This allows us to recover the ℓ_2 -regularized version of L_{Asim} :

We reiterate that both of the aforementioned objectives are special cases of the MAP formulation for the case of zero-mean isotropic Gaussian noise. Thus we expect that our method better handles non-Gaussian noise and experimentally confirm that our approach indeed leads to better reconstruction performance for noises with nonzero mean or conditional dependence across different pixel locations.

4 Theoretical Analysis

In this section we provide a theoretical analysis of our approach in two cases: denoising and compressed sensing. Unlike most prior work, we take a probabilistic approach and avoid making specific structural assumptions on the signal we want to recover, such as sparsity or being generated from a low-dimensional Gaussian prior.

For denoising, we show that better likelihood estimates lead to lower reconstruction error. For compressed sensing, we show that signals with higher density under the prior require fewer measurements to recover. Note that while our experiments employed flow models, our results apply to any likelihood-based generative model. Detailed proofs are provided in the appendix.

4.1 Recovery Guarantees for Denoising

Suppose we observe $\mathbf{y} = \mathbf{x}^* + \delta$ with Gaussian noise $\delta \sim \mathcal{N}(\mathbf{0}, \sigma^2 I)$ with $\|\delta\| = r$. We perform MAP inference by minimizing the following loss with gradient descent:

$$L_{\text{MAP}}(\mathbf{x}) = -\log p_{\Delta}(\mathbf{y} - \mathbf{x}) - \log p(\mathbf{x}) = \frac{1}{2\sigma^2} \|\mathbf{y} - \mathbf{x}\|^2 + q(\mathbf{x}), \quad (8)$$

where we write $q(\mathbf{x}) \triangleq -\log p(\mathbf{x})$ for notational convenience. Notice that the image we wish to recover is a natural image with high probability rather than an arbitrary one. Thus we consider the case where the ground truth image \mathbf{x}^* is a local maximum of p .

Theorem 4.1. *Let \mathbf{x}^* be a local optimum of the model $p(\mathbf{x})$ and $\mathbf{y} = \mathbf{x}^* + \delta$ be the noisy observation. Assume that q satisfies local strong convexity within the ball around \mathbf{x}^* defined as $B_r^d(\mathbf{x}^*) \triangleq \{\mathbf{x} \in \mathbb{R}^d : \|\mathbf{x} - \mathbf{x}^*\| \leq r\}$, i.e. the Hessian of q satisfies $H_q(\mathbf{x}) \succeq \mu I \forall \mathbf{x} \in B_r^d(\mathbf{x}^*)$ for some $\mu > 0$. Then gradient descent starting from \mathbf{y} on the loss function (8) converges to $\bar{\mathbf{x}}$, a local minimizer of $L_{\text{MAP}}(\mathbf{x})$, that satisfies:*

$$\|\bar{\mathbf{x}} - \mathbf{x}^*\| \leq \frac{1}{\mu\sigma^2 + 1} \|\delta\|$$

This theorem shows that a well-conditioned model with large μ leads to better denoising and confirms that our MAP formulation encourages reconstructions with high density. Thus, the maximum-likelihood training objective is directly aligned with better denoising performance.

4.2 Recovery Guarantees for Compressed Sensing

Here we show a worst-case bound for noisy compressed sensing where we observe $\mathbf{y} = A\mathbf{x}^* + \delta$ with noise level $\epsilon = \|\delta\|$ and $A \in \mathbb{R}^{m \times d}$ has entries drawn i.i.d. from $\mathcal{N}(0, 1/m)$. Note that the following constrained minimization problem is equivalent to the original unconstrained minimization of the loss in eq. (10) for a particular β via Lagrange multipliers.

Theorem 4.2. *For a given $\mathbf{x}^* \in \mathbb{R}^d$ and $\rho = \log p(\mathbf{x}^*)$, define $S(\rho) = \{\mathbf{x} \mid \log p(\mathbf{x}) \geq \rho\}$ to be the set of images with density higher than the ground truth image \mathbf{x}^* . Recall that the observation for \mathbf{x}^* is $\mathbf{y} = A\mathbf{x}^* + \delta$. When we perform the MAP inference by solving the following optimization problem,*

$$\bar{\mathbf{x}} \leftarrow \arg \min_{\mathbf{x} \in \mathbb{R}^d, \|A\mathbf{x} - \mathbf{y}\| \leq \epsilon} \{-\log p(\mathbf{x})\}, \quad (9)$$

we have:

$$\mathbb{E} \|\bar{\mathbf{x}} - \mathbf{x}^*\| \leq \sqrt{8\pi} \left(\frac{w(S(\rho))}{\sqrt{m}} + \epsilon \right),$$

where $w(\cdot)$ is the Gaussian mean width, and the expectation is over the randomness of A .

We note that in high dimensions, Gaussian mean width is on the same order as the size (i.e. the Lebesgue measure) of the set. Since the set $S(\rho)$ becomes smaller as ρ increases, this means the above error bound is tighter for ground truth images \mathbf{x}^* with higher density. In the extreme case where \mathbf{x}^* is the global maximum of the density function, we achieve zero recovery error.

5 Experiments

Our experiments are designed to test how well our MAP formulation performs in practice as we deviate from the commonly studied setting of linear inverse problems with Gaussian noise. Specifically, we focus on two aspects: (1) complex noise with dependencies and (2) non-linear forward operator. For all our experiments, we quantitatively evaluate each method by reporting peak signal-to-noise ratio (PSNR). We also visually inspect sample reconstructions for qualitative assessment.

Models: We trained multi-scale RealNVP models on two image datasets MNIST and CelebA-HQ [20, 21]. Due to computational constraints, all experiments were done on 100 randomly-selected images (1000 for MNIST) from the test set, as well as out-of-distribution images. A detailed description of the datasets, models and hyperparameters are provided in the appendix.

Baseline Methods: We compare our approach to the methods of [8] and [9], as they are two recently proposed approaches that use deep generative prior on inverse problems. Depending on the task, we also compare against BM3D [22], a popular off-the-shelf image denoising algorithm, and LASSO [23] with Discrete Cosine Transform (DCT) basis as appropriate. Note that for the 1-bit compressed sensing experiment, most existing techniques do not apply, since our task involves quantization as well as non-Gaussian noise.

We point out that the baselines methods are not designed to make use of the noise distribution, whereas our method does utilize it. Thus, the experiments are not meant to be taken as direct comparisons, but rather as an empirical evidence that the MAP formulation indeed benefits from the knowledge of noise structure.

Smoothing Parameter: Since our objective Equation (4) depends on the density $p_G(\mathbf{x})$ given by the flow model, our recovery of \mathbf{x} depends heavily on the quality of density estimates from the model. Unfortunately likelihood-based models exhibit counter-intuitive properties, such as assigning higher density on out-of-distribution examples or random noise over in-distribution examples. [24–27]. We empirically observe such behavior from our models as well. To remedy this, we use a smoothed version of the model density $p_G(x)^\beta$ where $\beta \geq 0$ is the *smoothing parameter*. Since the two extremes $\beta = 0$ and $\beta = \infty$ correspond to only using the noise density and the model density, respectively, β controls the degree to which we rely on p_G . Thus the loss we minimize becomes

$$L_G(\mathbf{z}; \mathbf{y}, \beta) = -\log p_\Delta(\mathbf{y} - f(G(\mathbf{z}))) - \beta \log p_G(G(\mathbf{z})) \quad (10)$$

5.1 Results

We test our methods on denoising and compressed sensing tasks that involve various structured, non-Gaussian noises as well as a non-linear forward operator. Note that many existing methods cannot be applied in this setting as they are designed for linear inverse problems and a specific noise model. While specialized algorithms do exist (e.g. for quantized compressed sensing), we note that our method is general and can be applied in a wide range of settings without modification.

5.1.1 Denoising MNIST Digits

The measurement process is $\mathbf{y} = 0.5 \cdot \mathbf{x} + \delta_{\text{MNIST}}$, where δ_{MNIST} represents MNIST digits added at different locations and color channels. Each digit itself comes from a flow model trained on the MNIST dataset. As shown in Figure 2, our method successfully removes MNIST noise. While the method of Bora et al. [8] also removes MNIST digits because its outputs are forced to be in the range of the DCGAN used, the

reconstructions are far from the ground truth – particularly on out-of-distribution samples that are not human faces.

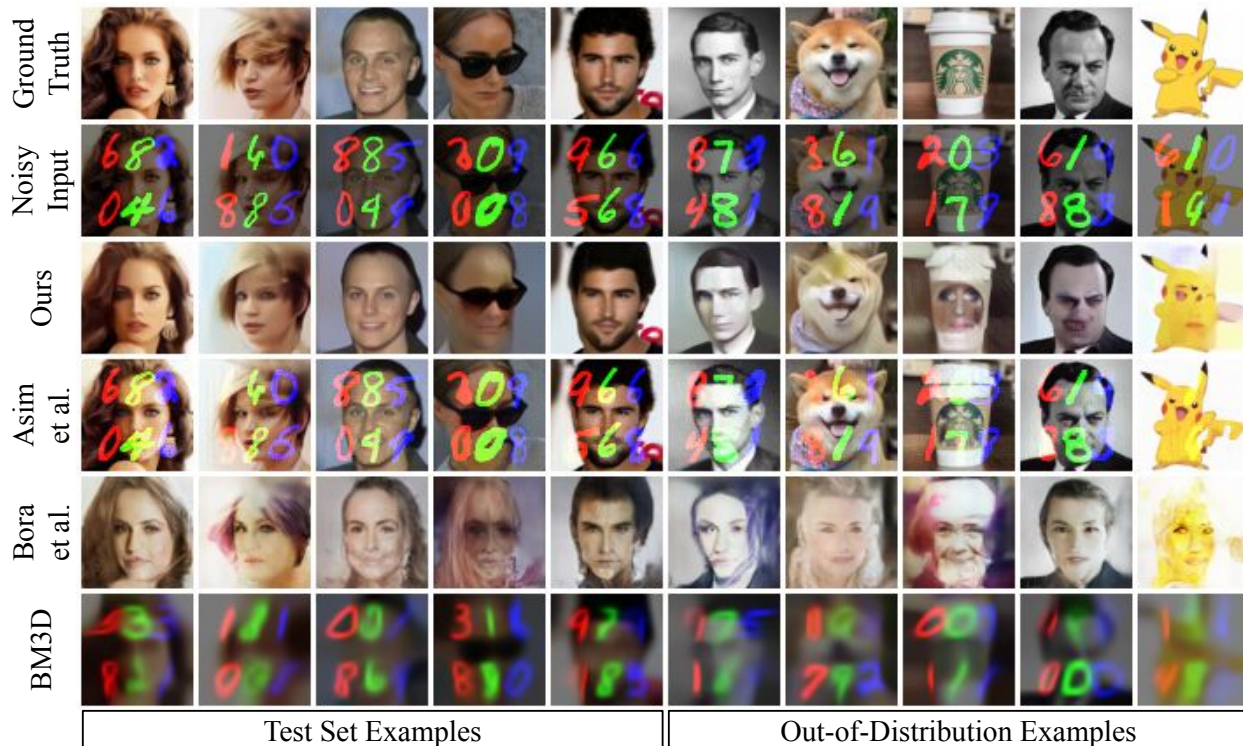


Figure 2: Result of removing MNIST noise from CelebA-HQ faces. Notice that without any understanding of the complex noise structure, baseline methods fail to produce good reconstructions.

5.1.2 Noisy Compressed Sensing

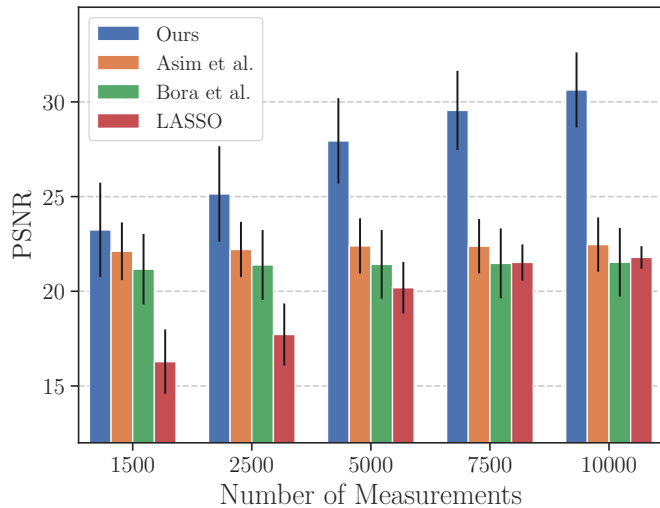
Now we consider the measurement process $\mathbf{y} = A\mathbf{x} + \delta_{\text{sine}}$ where $A \in \mathbb{R}^{m \times d}$ is a random Gaussian measurement matrix and δ has positive mean with variance that follows a sinusoidal pattern. Specifically, the k -th pixel of the noise has standard deviation $\sigma_k \propto \exp\left(\sin\left(\frac{2\pi k}{16}\right)\right)$ normalized to have the maximum variance of 1.

Figure 3a shows that our method is able to make a better use of additional measurements. Interestingly in Figure 3b, all three methods with deep generative prior produced plausible human faces. However, the reconstructions from Asim et al. [9] and Bora et al. [8] significantly differ from the ground truth images. We posit that this is due to the implicit Gaussian noise assumption made by the two methods, again showing the benefits of explicitly incorporating the knowledge of noise distribution.

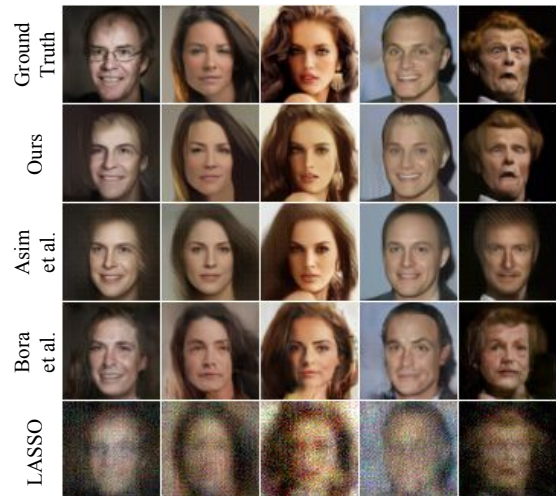
5.1.3 Removing SINUSOIDAL Noise

We consider another denoising task with observation $\mathbf{y} = \mathbf{x} + \delta_{\text{sine}}$. This is the 2-dimensional version of periodic noise, where the noise variance for all pixels within the k -th row follows σ_k from above.

From Figure 4 and Figure 5a, we see that baseline methods do not perform well even though the noise is simply Gaussian at each pixel. This reemphasizes an important point: without an understanding of the *structure* of the noise, algorithms designed to handle Gaussian noise have difficulty removing them when we introduce variability across different pixel locations.



(a) PSNR at different measurement counts (best viewed in color). The approaches by Asim et al. [9] and Bora et al. [8] show little improvements from having more measurements due to their inability to take the noise model into account.



(b) Reconstructions at 2500 measurements. Notice that even though existing approaches produce reconstructions that resemble human faces, they do not match the ground truth as well as our method.

Figure 3: Experiment results for noisy compressed sensing on CelebA-HQ images.

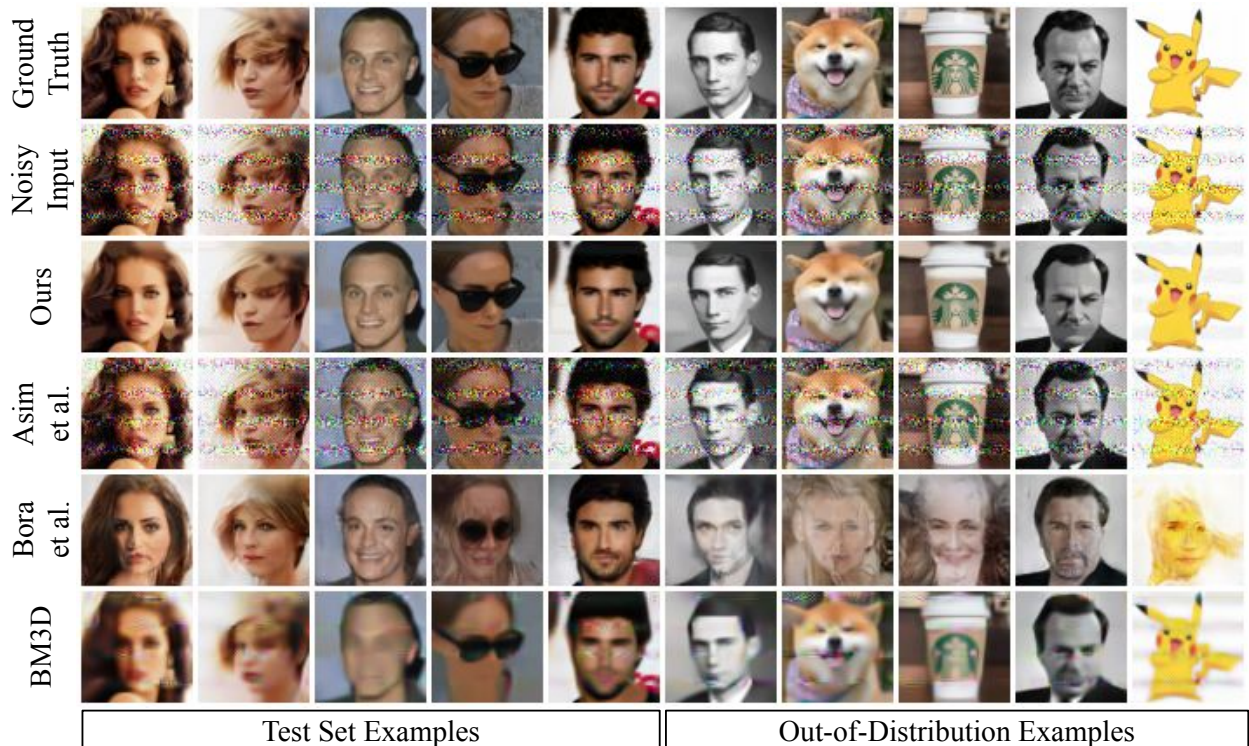
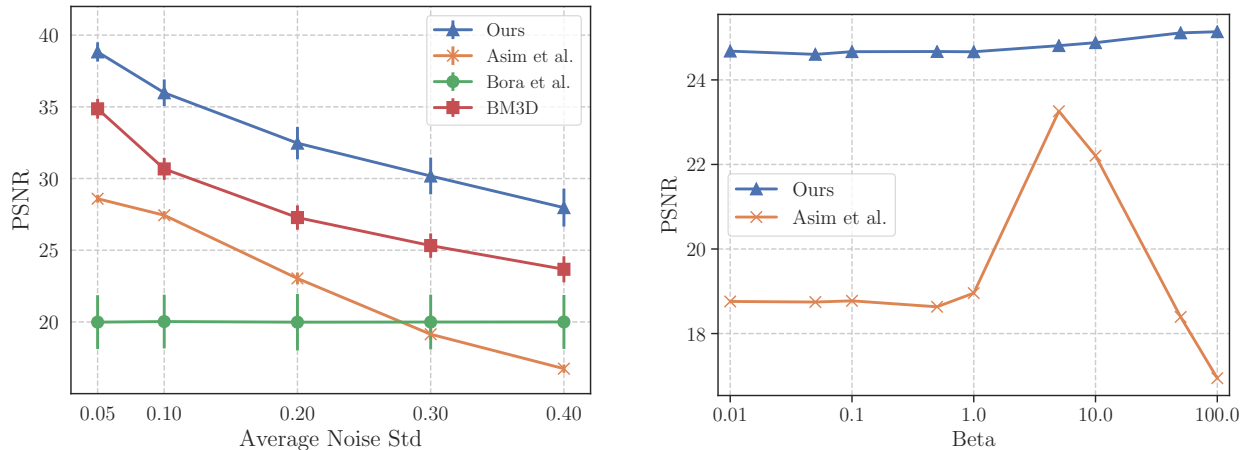


Figure 4: Result of denoising SINUSOIDAL noise on CelebA-HQ faces and out-of-distribution images.

5.1.4 Noisy 1-bit Compressed Sensing

This task considers a combination of a non-linear forward operator as well as a non-Gaussian noise. The measurement process is $\mathbf{y} = \text{sign}(A\mathbf{x}) + \delta_{\text{sin}}$, identical to noisy compressed sensing except with the sign function. This is the most extreme case of quantized compressed sensing, since \mathbf{y} only contains the (noisy)



(a) Result for SINUSOIDAL denoising on CelebA-HQ images at various noise rates. Our method achieves the same reconstruction performance even when the noise has up to $3\times$ higher average standard deviation compared to the best baseline method (BM3D).

(b) Compressed sensing performance of our method and [9] at different hyperparameter values. For our method, we vary the smoothing parameter β in L_G . For Asim et al. [9], we vary the regularization coefficient γ in L_{Asim} .

Figure 5: SINUSOIDAL denoising results (left) and hyperparameter sensitivity plot (right).

sign $\{+1, -1\}$ of the measurements. Because the gradient of sign function is zero everywhere, we use Straight-Through Estimator [28] for backpropagation. See Figure 6a and Figure 6b for a comparison of our method to the baselines at varying numbers of measurements.

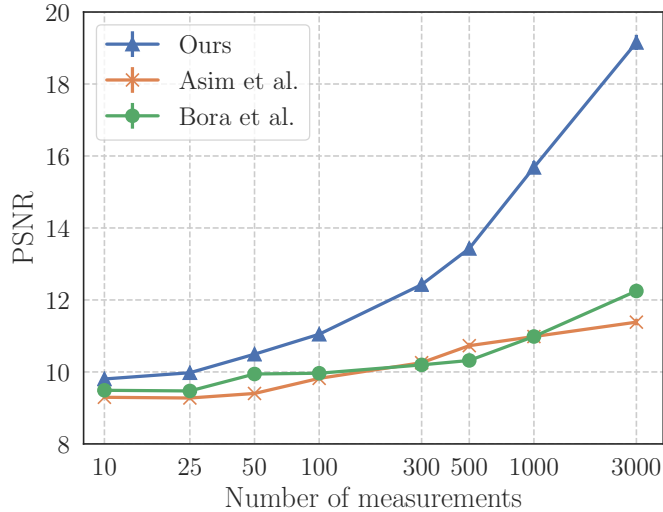
5.1.5 Sensitivity to Hyperparameters

We also observe that our method is more robust to hyperparameter choices than [9], as shown in Figure 5b. This may come as a surprise given that our objective has an additional log-determinant term. We speculate that this is due to the regularization term in $L_{\text{Asim}}(\mathbf{z}; \mathbf{y}) = \|\mathbf{y} - f(G(\mathbf{z}))\|^2 + \gamma \|\mathbf{z}\|$.

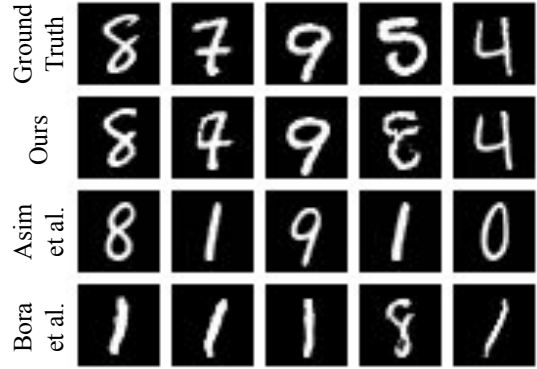
It is known that samples from d -dimensional isotropic Gaussian concentrate around a thin “shell” around the sphere of radius \sqrt{d} . This suggests that the range of $\|\mathbf{z}\|$ corresponding to natural images may be small. Thus, forcing the latent variable \mathbf{z} to have small norm without taking the log-determinant term into account could lead to a sudden drop in the reconstruction quality.

6 Conclusion

We propose a novel method to solve inverse problems for general differentiable forward operators and structured noise. Our method generalizes that of [9] to arbitrary differentiable forward operators and non-Gaussian noise distributions. The power of our approach stems from the flexibility of invertible generative models which can be combined in a modular way to solve MAP inverse problems in very general settings, as we demonstrate. The central theoretical question that remains open is to analyze the optimization problem we formulated. In this paper we empirically minimize this loss using gradient descent, but some theoretical guarantees would be desirable, possibly under assumptions, e.g. random weights following the framework of [29].



(a) Result of 1-bit noisy compressed sensing at different measurement counts. Our method achieves the same reconstruction performance using up to $2\times$ fewer measurements compared to the best baseline method [9].



(b) Reconstructions from noisy 1-bit compressed sensing with 3000 binary measurements. Notice that our method fails more gracefully compared to other methods, i.e. even when the reconstructions differ from the ground truth, substantial parts of the reconstructions are still correct. On the other hand, other methods predict a completely different digit.

Figure 6: Results of 1-bit compressed sensing experiments.

Acknowledgements

This research has been supported by NSF Grants 1618689, DMS 1723052, CCF 1763702, AF 1901292 and research gifts by Google, Western Digital and the Fluor Centennial Teaching Fellowship.

References

- [1] Emmanuel J Candes, Justin K Romberg, and Terence Tao. Stable signal recovery from incomplete and inaccurate measurements. *Communications on pure and applied mathematics*, 59(8):1207–1223, 2006.
- [2] David L Donoho. Compressed sensing. *IEEE Transactions on information theory*, 52(4):1289–1306, 2006.
- [3] Guang-Hong Chen, Jie Tang, and Shuai Leng. Prior image constrained compressed sensing (piccs): a method to accurately reconstruct dynamic ct images from highly undersampled projection data sets. *Medical physics*, 35 2:660–3, 2008.
- [4] Michael Lustig, David Donoho, and John M Pauly. Sparse mri: The application of compressed sensing for rapid mr imaging. *Magnetic Resonance in Medicine: An Official Journal of the International Society for Magnetic Resonance in Medicine*, 58(6):1182–1195, 2007.
- [5] Emmanuel J Candes, Yonina C Eldar, Thomas Strohmer, and Vladislav Voroninski. Phase retrieval via matrix completion. *SIAM review*, 57(2):225–251, 2015.
- [6] Emmanuel J Candes, Xiaodong Li, and Mahdi Soltanolkotabi. Phase retrieval via wirtinger flow: Theory and algorithms. *IEEE Transactions on Information Theory*, 61(4):1985–2007, 2015.
- [7] Richard G Baraniuk, Volkan Cevher, Marco F Duarte, and Chinmay Hegde. Model-based compressive sensing. *IEEE Transactions on information theory*, 56(4):1982–2001, 2010.
- [8] Ashish Bora, Ajil Jalal, Eric Price, and Alexandros G Dimakis. Compressed sensing using generative models. In *Proceedings of the 34th International Conference on Machine Learning-Volume 70*, pages 537–546. JMLR. org, 2017.

- [9] Muhammad Asim, Ali Ahmed, and Paul Hand. Invertible generative models for inverse problems: mitigating representation error and dataset bias. *CoRR*, abs/1905.11672, 2019. URL <http://arxiv.org/abs/1905.11672>.
- [10] Dave Van Veen, Ajil Jalal, Mahdi Soltanolkotabi, Eric Price, Sriram Vishwanath, and Alexandros G Dimakis. Compressed sensing with deep image prior and learned regularization. *arXiv preprint arXiv:1806.06438*, 2018.
- [11] George Papamakarios, Eric Nalisnick, Danilo Jimenez Rezende, Shakir Mohamed, and Balaji Lakshminarayanan. Normalizing flows for probabilistic modeling and inference. *arXiv preprint arXiv:1912.02762*, 2019.
- [12] Esteban G Tabak and Cristina V Turner. A family of nonparametric density estimation algorithms. *Communications on Pure and Applied Mathematics*, 66(2):145–164, 2013.
- [13] Ian Goodfellow, Jean Pouget-Abadie, Mehdi Mirza, Bing Xu, David Warde-Farley, Sherjil Ozair, Aaron Courville, and Yoshua Bengio. Generative adversarial nets. In *Advances in neural information processing systems*, pages 2672–2680, 2014.
- [14] Diederik P Kingma and Max Welling. Auto-encoding variational bayes. *arXiv preprint arXiv:1312.6114*, 2013.
- [15] Manik Dhar, Aditya Grover, and Stefano Ermon. Modeling sparse deviations for compressed sensing using generative models, 2018.
- [16] Viraj Shah and Chinmay Hegde. Solving linear inverse problems using gan priors: An algorithm with provable guarantees. In *2018 IEEE International Conference on Acoustics, Speech and Signal Processing (ICASSP)*, pages 4609–4613. IEEE, 2018.
- [17] Dmitry Ulyanov, Andrea Vedaldi, and Victor Lempitsky. Deep image prior. In *Proceedings of the IEEE Conference on Computer Vision and Pattern Recognition*, pages 9446–9454, 2018.
- [18] Yan Wu, Mihaela Rosca, and Timothy P. Lillicrap. Deep compressed sensing. *CoRR*, abs/1905.06723, 2019. URL <http://arxiv.org/abs/1905.06723>.
- [19] Lynton Ardizzone, Jakob Kruse, Sebastian J. Wirkert, Daniel Rahner, Eric W. Pellegrini, Ralf S. Klessen, Lena Maier-Hein, Carsten Rother, and Ullrich Köthe. Analyzing inverse problems with invertible neural networks. *CoRR*, abs/1808.04730, 2018. URL <http://arxiv.org/abs/1808.04730>.
- [20] Yann LeCun, Léon Bottou, Yoshua Bengio, and Patrick Haffner. Gradient-based learning applied to document recognition. *Proceedings of the IEEE*, 86(11):2278–2324, 1998.
- [21] Ziwei Liu, Ping Luo, Xiaogang Wang, and Xiaoou Tang. Deep learning face attributes in the wild. In *Proceedings of International Conference on Computer Vision (ICCV)*, December 2015.
- [22] Kostadin Dabov, Alessandro Foi, Vladimir Katkovnik, and Karen Egiazarian. Image denoising with block-matching and 3d filtering. In *Image Processing: Algorithms and Systems, Neural Networks, and Machine Learning*, volume 6064, page 606414. International Society for Optics and Photonics, 2006.
- [23] Robert Tibshirani. Regression shrinkage and selection via the lasso. *Journal of the Royal Statistical Society: Series B (Methodological)*, 58(1):267–288, 1996.
- [24] Eric Nalisnick, Akihiro Matsukawa, Yee Whye Teh, Dilan Gorur, and Balaji Lakshminarayanan. Do deep generative models know what they don’t know? *arXiv preprint arXiv:1810.09136*, 2018.
- [25] Hyunsun Choi, Eric Jang, and Alexander A Alemi. Waic, but why? generative ensembles for robust anomaly detection. *arXiv preprint arXiv:1810.01392*, 2018.

- [26] Dan Hendrycks and Thomas G Dietterich. Benchmarking neural network robustness to common corruptions and surface variations. *arXiv preprint arXiv:1807.01697*, 2018.
- [27] Eric Nalisnick, Akihiro Matsukawa, Yee Whye Teh, and Balaji Lakshminarayanan. Detecting out-of-distribution inputs to deep generative models using a test for typicality. *arXiv preprint arXiv:1906.02994*, 2019.
- [28] Yoshua Bengio, Nicholas Léonard, and Aaron Courville. Estimating or propagating gradients through stochastic neurons for conditional computation. *arXiv preprint arXiv:1308.3432*, 2013.
- [29] Paul Hand and Vladislav Voroninski. Global guarantees for enforcing deep generative priors by empirical risk. *IEEE Transactions on Information Theory*, 2020.
- [30] Roman Vershynin. Estimation in high dimensions: a geometric perspective. In *Sampling theory, a renaissance*, pages 3–66. Springer, 2015.
- [31] Durk P Kingma and Prafulla Dhariwal. Glow: Generative flow with invertible 1x1 convolutions. In *Advances in Neural Information Processing Systems*, pages 10215–10224, 2018.
- [32] Laurent Dinh, Jascha Sohl-Dickstein, and Samy Bengio. Density estimation using real nvp. *arXiv preprint arXiv:1605.08803*, 2016.

A Omitted Proofs

A.1 Proof for Denoising

Proof of Theorem 4.1. We first show that gradient descent with sufficiently small learning rate will converge to $\bar{\mathbf{x}}$, the locally-optimal solution of Equation (8). Recall the loss function $L(\mathbf{x}) := q(\mathbf{x}) + \frac{1}{2\sigma^2}\|\mathbf{x} - \mathbf{y}\|^2$ (we subsume the scaling $\frac{1}{2}$ into $\frac{1}{\sigma^2}$ without loss of generality). Notice in the ball $B_r^d(\mathbf{x}^*) := \{\mathbf{x} \in \mathbb{R}^d \mid \|\mathbf{x} - \mathbf{x}^*\| \leq r\}$, L is $(\mu + \frac{1}{\sigma^2})$ strongly-convex. We next show there is a stationary point $\bar{\mathbf{x}} \in B_r^d(\mathbf{x}^*)$ of $L(\mathbf{x})$.

$$\begin{aligned} \nabla L(\bar{\mathbf{x}}) = 0 &\implies \nabla q(\bar{\mathbf{x}}) + \frac{1}{\sigma^2}(\bar{\mathbf{x}} - \mathbf{y}) = 0 \\ &\implies \nabla q(\bar{\mathbf{x}}) - \nabla q(\mathbf{x}^*) = \frac{1}{\sigma^2}(\mathbf{y} - \bar{\mathbf{x}}) \\ &\implies \langle \nabla q(\bar{\mathbf{x}}) - \nabla q(\mathbf{x}^*), \bar{\mathbf{x}} - \mathbf{x}^* \rangle = \frac{1}{\sigma^2} \langle \mathbf{y} - \bar{\mathbf{x}}, \bar{\mathbf{x}} - \mathbf{x}^* \rangle \end{aligned}$$

From strong convexity of q , $\langle \nabla q(\bar{\mathbf{x}}) - \nabla q(\mathbf{x}^*), \bar{\mathbf{x}} - \mathbf{x}^* \rangle \geq \mu \|\bar{\mathbf{x}} - \mathbf{x}^*\|^2$. Thus

$$\begin{aligned} \frac{1}{\sigma^2} \langle \mathbf{y} - \mathbf{x}^*, \bar{\mathbf{x}} - \mathbf{x}^* \rangle &= \frac{1}{\sigma^2} \langle (\mathbf{y} - \bar{\mathbf{x}}) + (\bar{\mathbf{x}} - \mathbf{x}^*), \bar{\mathbf{x}} - \mathbf{x}^* \rangle \\ &= \frac{1}{\sigma^2} \langle \mathbf{y} - \bar{\mathbf{x}}, \bar{\mathbf{x}} - \mathbf{x}^* \rangle + \frac{1}{\sigma^2} \langle \bar{\mathbf{x}} - \mathbf{x}^*, \bar{\mathbf{x}} - \mathbf{x}^* \rangle \\ &= \langle \nabla q(\bar{\mathbf{x}}) - \nabla q(\mathbf{x}^*), \bar{\mathbf{x}} - \mathbf{x}^* \rangle + \frac{1}{\sigma^2} \|\bar{\mathbf{x}} - \mathbf{x}^*\|^2 \\ &\geq \mu \|\bar{\mathbf{x}} - \mathbf{x}^*\|^2 + \frac{1}{\sigma^2} \|\bar{\mathbf{x}} - \mathbf{x}^*\|^2 \\ &= \left(\mu + \frac{1}{\sigma^2} \right) \|\bar{\mathbf{x}} - \mathbf{x}^*\|^2 \end{aligned}$$

Finally, by Cauchy-Schwartz inequality $\langle \mathbf{y} - \mathbf{x}^*, \bar{\mathbf{x}} - \mathbf{x}^* \rangle \leq \|\mathbf{y} - \mathbf{x}^*\| \cdot \|\bar{\mathbf{x}} - \mathbf{x}^*\|$. So we get $\|\bar{\mathbf{x}} - \mathbf{x}^*\| \leq \frac{1}{1+\mu\sigma^2} \|\mathbf{y} - \mathbf{x}^*\| \leq \|\boldsymbol{\delta}\| \leq r$, i.e., $\bar{\mathbf{x}} \in B_r^d(\mathbf{x}^*)$. Notice L is $(\mu + \frac{1}{\sigma^2})$ strongly-convex in $B_r^d(\mathbf{x}^*)$, which contains the stationary point $\bar{\mathbf{x}}$. Therefore $\bar{\mathbf{x}}$ is a local minimizer of $L(\mathbf{x})$. Also note that we implicitly require q to be twice differentiable, meaning in a compact set $B_r^d(\mathbf{x}^*)$ its smoothness is upper bounded by a constant M . Thus gradient descent starting from $\mathbf{y} \in B_r^d(\mathbf{x}^*)$ with learning rate smaller than $\frac{1}{M}$ will converge to $\bar{\mathbf{x}}$ without leaving the (convex) set $B_r^d(\mathbf{x}^*)$. \square

A.2 Proof for Compressed sensing

Definition A.1 (Gaussian mean width). *The Gaussian mean width of a set $K \subset \mathbb{R}^d$ is defined as:*

$$w(K) \triangleq \mathbb{E}_{\mathbf{g} \sim \mathcal{N}(0, I_d)} \left[\sup_{\mathbf{x} \in M(K)} |\langle \mathbf{g}, \mathbf{x} \rangle| \right],$$

where $M(K) = \{\mathbf{x} - \mathbf{y} : \mathbf{x}, \mathbf{y} \in K\}$ is the Minkowski sum of K and $-K$.

Intuitively, Gaussian mean width measures the complexity of the set K .

Theorem A.2 (Adapted from Theorem 6.1 by Vershynin [30]). *Let $K \subset \mathbb{R}^d$ be an arbitrary bounded set, and $A \in \mathbb{R}^{m \times d}$ be a random matrix with its entries sampled iid from Gaussian distribution $\mathcal{N}(0, 1)$, observation $\mathbf{y} = A\mathbf{x}^* + \boldsymbol{\delta}$, where $\frac{1}{\sqrt{m}}\|\boldsymbol{\delta}\|_2 = \epsilon$, and \mathbf{x}^* is unknown. Choose $\hat{\mathbf{x}}$ to be any vector satisfying $\hat{\mathbf{x}} \in K$ and $\frac{1}{\sqrt{m}}\|A\hat{\mathbf{x}} - \mathbf{y}\|_2 \leq \epsilon$. Then*

$$\mathbb{E} \left[\sup_{\hat{\mathbf{x}} \in K} \|\hat{\mathbf{x}} - \mathbf{x}^*\|_2 \right] \leq \sqrt{8\pi} \left(\frac{w(K)}{\sqrt{m}} + \epsilon \right). \quad (11)$$

One consequence of this theorem is that $m = \Theta(w(K)^2)$ measurements are sufficient to guarantee small recovery error.

Remark: The statement of Theorem A.2 is only different from the original Theorem 6.1 in [30] where we replaced the ℓ_1 norm assumption by a stronger ℓ_2 norm assumption, and therefore is a slightly weaker version of the original theorem. As indicated in [30], this is still valid. To see this, notice that for any $\hat{\delta} \in \mathbb{R}^m$, we have $\|\hat{\delta}\|_1 \leq \sqrt{m} \|\hat{\delta}\|_2$. So the ℓ_2 bound $\frac{1}{\sqrt{m}} \|\hat{\delta}\|_2 \leq \epsilon$ gives $\frac{1}{m} \|\hat{\delta}\|_1 \leq \frac{1}{\sqrt{m}} \|\hat{\delta}\|_2 \leq \epsilon$.

Theorem A.3 (Restatement of Theorem 4.2). *For a given \mathbf{x}^* and $q = \log p(\mathbf{x}^*)$, define $S(q) = \{\mathbf{x} \mid \log p(\mathbf{x}) \geq q\}$. Recall that the observation for \mathbf{x}^* is $\mathbf{y} = A\mathbf{x}^* + \delta$ where $A \in \mathbb{R}^{m \times d}$ has entries drawn i.i.d. from $\mathcal{N}(0, 1/m)$ and the noise level is $\epsilon = \|\delta\|_2$. When we perform the MAP inference by solving the following problem,*

$$\bar{\mathbf{x}} \leftarrow \arg \min_{\mathbf{x} \in \mathbb{R}^d, \|A\mathbf{x} - \mathbf{y}\|_2 \leq \epsilon} \{-\log p(\mathbf{x})\}, \quad (12)$$

we have:

$$\mathbb{E} \|\bar{\mathbf{x}} - \mathbf{x}^*\|_2 \leq \sqrt{8\pi} \left(\frac{w(S(q))}{\sqrt{m}} + \epsilon \right),$$

where the expectation is over the randomness of A .

Proof. Since $\mathbb{E} \|\bar{\mathbf{x}} - \mathbf{x}^*\|_2 \leq \mathbb{E} \left[\sup_{\mathbf{x} \in S(q)} \|\bar{\mathbf{x}} - \mathbf{x}\|_2 \right]$, the proof directly follows from Theorem A.2 by choosing the set K to be $S(q)$. We only need to verify that $\bar{\mathbf{x}}$ is indeed inside $S(q)$. Notice that both $\bar{\mathbf{x}}$ and \mathbf{x}^* are in the feasible set $\{\mathbf{x} : \|A\mathbf{x} - \mathbf{y}\|_2 \leq \epsilon\}$. Since $\bar{\mathbf{x}}$ maximizes $\log p(\mathbf{x})$ within this set, clearly its density should be at least that of \mathbf{x}^* , i.e. $\log p(\bar{\mathbf{x}}) \geq \log p(\mathbf{x}^*) = q$. Thus $\bar{\mathbf{x}} \in S(q)$.

Note that in our setting the variance of A 's entries is set to be $1/m$ instead of 1 from Theorem A.2. Since the Gaussian mean width $w(S(q))$ is invariant to the scaling of A , we correct the scaling on the noise term and obtain $\mathbb{E} \left[\sup_{\mathbf{x} \in S(q)} \|\bar{\mathbf{x}} - \mathbf{x}^*\|_2 \right] \leq \sqrt{8\pi} \left(\frac{w(S(q))}{\sqrt{m}} + \epsilon \right)$. \square

Remark: Here we show the recovery guarantee when we optimize over the constrained version as in eq. (12). Note that for a suitable constant β , the constrained version $\min_{\mathbf{x}: \|A\mathbf{x} - \mathbf{y}\|_2 \leq \epsilon} \{-\log p(\mathbf{x})\}$ is equivalent to $\min_{\mathbf{x}} \{-\log p(\mathbf{x}) + \beta \|A\mathbf{x} - \mathbf{y}\|_2^2\}$.

B Additional Experimental Results and Details

Here we include experimental results and details not included in the main text. Across all the experiments, we individually tuned the hyperparameters for each method.

B.1 Experimental Details

Dataset For MNIST, we used the default split of 60,000 training images and 10,000 test images of [20]. For CelebA-HQ, we used the split of 27,000 training images and 3,000 test images as provided by [31]. During evaluation, the following Python script was used to select 1000 MNIST images and 100 CelebA-HQ images from their respective test sets:

```
np.random.seed(0); indices_mnist = np.random.choice(10000, 1000, False)
np.random.seed(0); indices_celeba = np.random.choice(3000, 100, False)
```

Note that CelebA-HQ images were further resized to 64×64 resolution.

Noise Distribution For the sinusoidal noise used in the experiments, the standard deviation of the k -th pixel/row is calculated as: $\sigma_k = 0.1 \cdot \left(\exp \left(\sin \left(2\pi \cdot \frac{k}{16} \right) \right) - 1 \right) / (e - 1)$, clamped to be in range $[0.001, 1]$. For Figure 8b, we used vary the coefficient 0.1 to values in $\{0.05, 0.1, 0.2, 0.3, 0.4\}$.

For the radial noise used in the additional experiment below, the standard deviation of each pixel with ℓ_2 distance is d from the center pixel (31, 31) is computed as: $\sigma_k = 0.1 \cdot \exp(-0.005 \cdot d^2)$, clamped to be in range [0.001, 1000].

B.2 Additional Result: Removing RADIAL Noise

Consider the measurement process $\mathbf{y} = \mathbf{x} + \delta_{\text{radial}}$, where each pixel follows a Gaussian distribution, but with variance that decays exponentially in distance to the center point. For a pixel whose ℓ_2 distance to the center pixel is d , the standard deviation is computed as $\sigma(d) = \exp(-0.005 \cdot d^2)$. See Figure 7 and Figure 8a for reconstructions as well as PSNR plot comparing the methods considered.

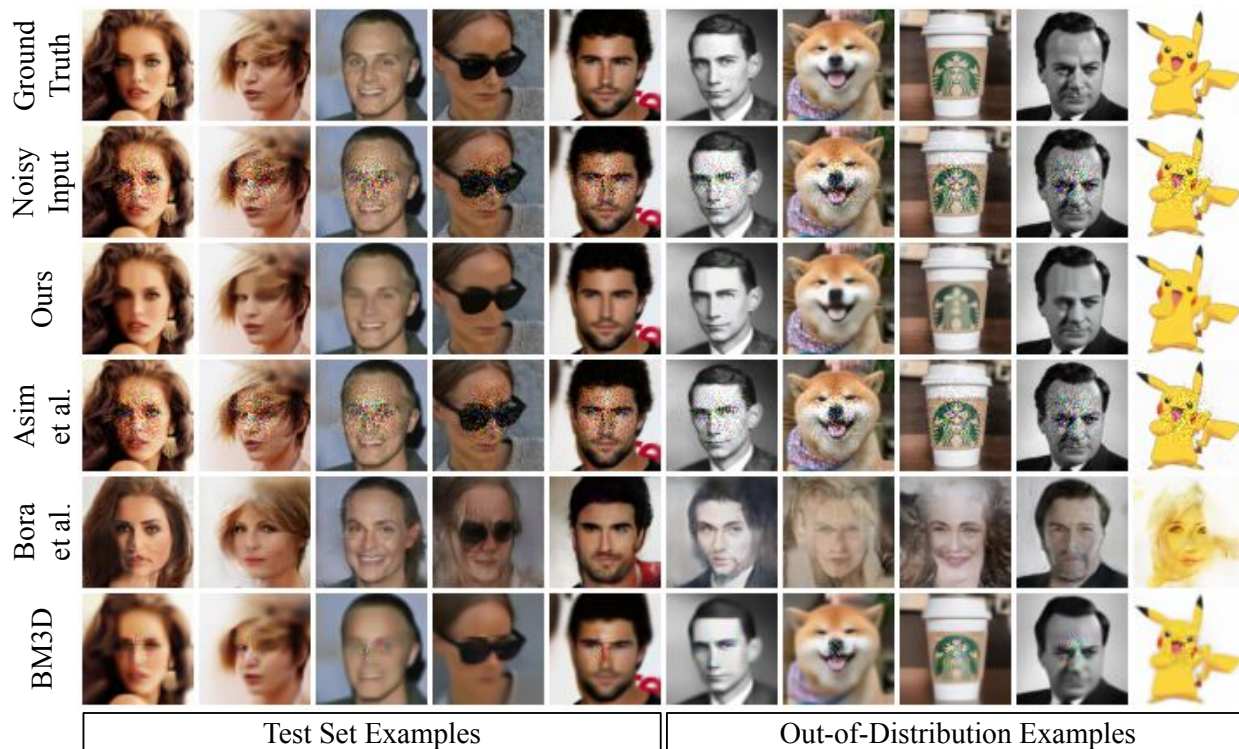


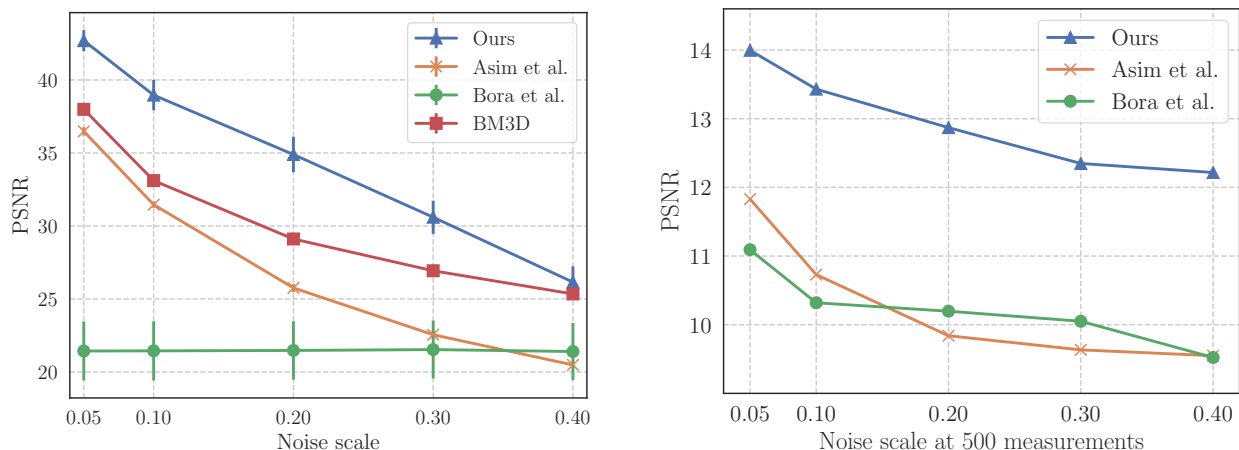
Figure 7: Result of denoising RADIAL noise on CelebA-HQ faces and out-of-distribution images.

B.3 Additional Result: 1-bit Compressed Sensing

Figure 8b shows the performance of each method at different noise scales for a fixed number of measurements. We observe that our method performs consistently better at all noise levels.

C Model Architecture and Hyperparameters

For the RealNVP models we trained, we used multiscale architecture as was done in [32], with residual networks and regularized weight normalization on convolutional layers. Following [31], we used 5-bit color depth for the CelebA-HQ model. Hyperparameters and samples from the models can be found in Table 1 and Figure 9.



(a) Result on denoising RADIAL noise at varying noise rates. Our method achieves the same reconstruction performance even when the noise has approximately $1.5\times$ higher noise scale compared to the best baseline method which is BM3D for this setting.

(b) Result of 1-bit compressed sensing at different noise scale. Our method obtains the best reconstructions, achieving similar PSNR as [9] when the noise scale is $8\times$ higher.

Figure 8: RADIAL denoising results (left) and 1-bit compressed sensing results at different noise levels (right).

Hyperparameter	CelebA-HQ	MNIST
Learning rate	$5e-4$	$1e-3$
Batch size	16	128
Image size	$64 \times 64 \times 3$	$28 \times 28 \times 1$
Pixel depth	5 bits	8 bits
Number of epochs	300	200
Number of scales	6	3
Residual blocks per scale	10	6
Learning rate halved every	60 epochs	40 epochs
Max gradient norm	500	100
Weightnorm regularization	$1e-5$	$5e-5$

Table 1: Hyperparameters used for RealNVP models.

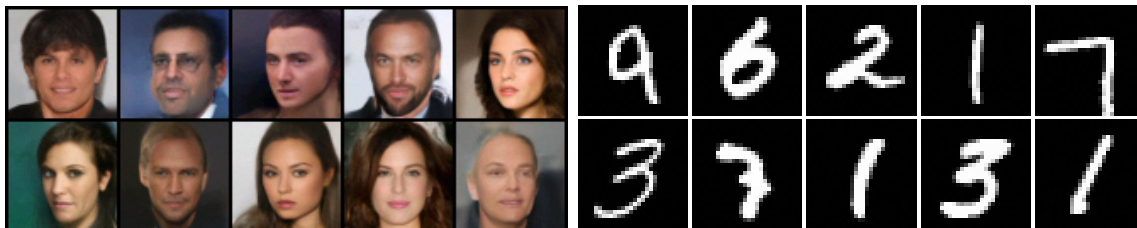


Figure 9: Samples from the RealNVP models used in our experiments.



Figure 10: Out-of-distribution images used in our experiments. We included different types of out-of-distribution instances including greyscale images and cartoons with flat image areas.